JACS
JOURNAL OF THE AMERICAN CHEMICAL SOCIETY

Article

pubs.acs.org/JACS

Retrosynthetic Analysis-Guided Breaking Tile Symmetry for the Assembly of Complex DNA Nanostructures

Pengfei Wang,[†] Siyu Wu,[‡] Cheng Tian,[‡] Guimei Yu,[§] Wen Jiang,[§] Guansong Wang,*[,∥] and Chengde Mao*[,‡]

[†]Weldon School of Biomedical Engineering, [‡]Department of Chemistry, and [§]Markey Center for Structural Biology and Department of Biological Sciences, Purdue University, West Lafayette Indiana 47907, United States

[∥]Institute of Respiratory Diseases, Xinqiao Hospital, Chongqing 400037, China

Supporting Information

ABSTRACT: Current tile-based DNA self-assembly produces simple repetitive or highly symmetric structures. In the case of 2D lattices, the unit cell often contains only one basic tile because the tiles often are symmetric (in terms of either the backbone or the sequence). In this work, we have applied retrosynthetic analysis to determine the minimal asymmetric units for complex DNA nanostructures. Such analysis guides us to break the intrinsic structural symmetries of the tiles to achieve high structural complexities. This strategy has led to the construction of several DNA nanostructures that are not accessible from conventional symmetric tile designs. Along with previous studies, herein we have established a set of four fundamental rules regarding tile-based assembly. Such rules could serve as guidelines for the design of DNA nanostructures.

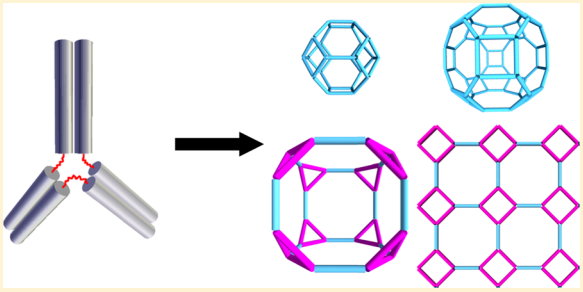

INTRODUCTION

Programmed DNA self-assembly has been demonstrated to have an unprecedented capability of constructing artificial nanostructures with prescribed sizes, shapes, and functions.[1] These as-assembled nanostructures have been utilized for numerous applications, such as nanoplasmonics[2−4] and drug delivery.[5−11] Though DNA origami[12−19] and DNA bricks[20−22] could potentially construct 2D or 3D structures with virtually any desired size and shape, they routinely require hundreds of DNA strands of unique sequences. An alternative, cost-effective approach is DNA motif (tile)-based assembly, which consists of only a few (<10) unique strands. Sticky-end-mediated assembly of the motif has produced 1D,[23−26] 2D,[27−34] and 3D[35−44] structures with well-defined patterns. Such motifs often contain intrinsic structural symmetries (in terms of DNA backbones). Imposing such symmetries on the DNA sequences can further reduce the number of unique component strands. We have previously utilized symmetric DNA motifs to construct a variety of DNA nanostructures. For complex DNA nanostructures, retrosynthetic analysis indicates that the basic DNA motifs have to be asymmetric in the backbones and sequences. By breaking the structural symmetries, DNA motifs are expected to assemble into more complex structures. For instance, a family of triangular prisms with controlled chirality have been fabricated by using asymmetric three-point-star motifs.[42] More recently, complex 2D lattices were assembled from multiple asymmetric point-star motifs,[34] though multiple, different motifs were used. Herein, we have greatly expanded this strategy via rationally designing the motif branch, flexibility, asymmetry, and DNA concentration to control the self-assembly of complex 2D and 3D structures from a single-component, three-point-star motif. More importantly, we have established a set of four basic rules for tile-based DNA self-assembly, which are expected to guide the design of DNA nanostructures.

DESIGN OF DNA MOTIFS

Three types of motifs are designed in this study: Motif-O, Motif-EOE, and Motif-E (Figure 1a). Each motif consists of seven strands: one central, long strand (C; blue/red), three medium strands (M; green), and three short strands (S; black). In the assembled motif, strand C contains three red, single-stranded loops (L1, L2, and L3). The loop length (0 to 7 bases long) controls the flexibility and asymmetry of the motif. Upon tile association (Figure 1b), neighboring Motif-Os alternatively face up and down because the edge (O-edge) connecting two Motif-Os is an odd number of helical half-turns (4.5 turns) long. The edges (E-edge) formed between Motif-Es are an even number of helical half-turns (4 turns) long. Motif-EOE is a hybrid design of Motif-O and Motif-E with two branches forming E-edges and one branch forming an O-edge. To guide the design of DNA nanostructures via tile-based self-assembly, a set of rules is derived from previous studies (Figure 1c−f) and verified in the current study. On the basis of these rules, we have constructed a series of moderately complex DNA

Received: June 13, 2016
Published: October 11, 2016

DOI: 10.1021/jacs.6b06074
J. Am. Chem. Soc. 2016, 138, 13579−13585

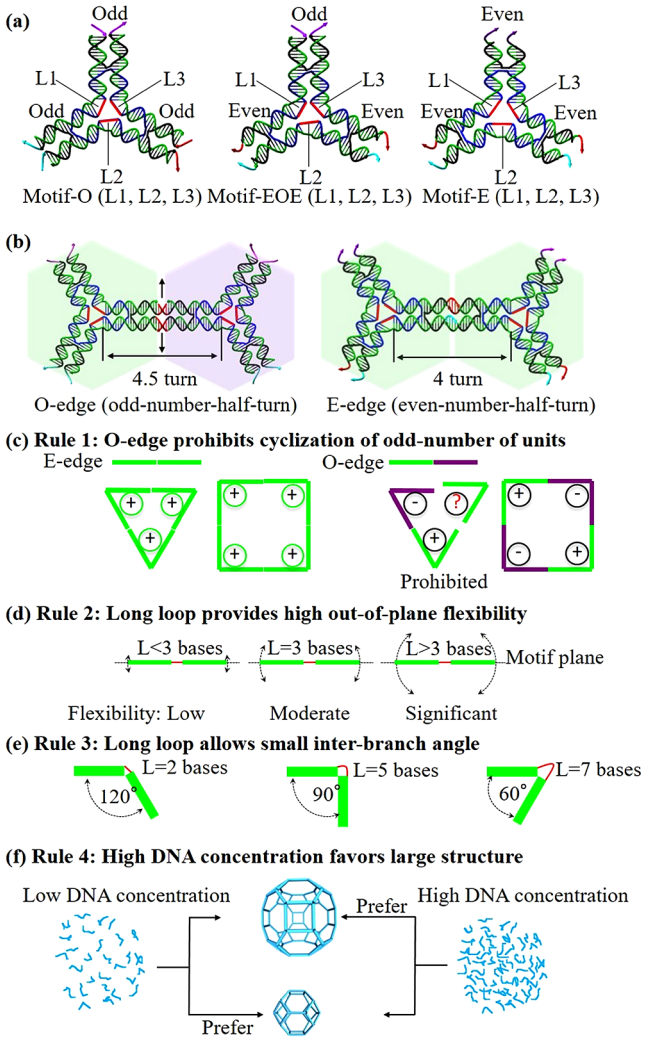

Figure 1. (a) Schematics of three asymmetric three-point-star DNA motifs. Motif-O: each branch is 2.25 turns long and has self-complementary sticky ends. Motif-EOE: the two bottom branches are 2 turns long and have complementary sticky ends; the top branch is 2.25 turns long and has self-complementary sticky ends. Motif-E: each branch is 2 turns long; the two bottom branches have complementary sticky ends; the top branch has self-complementary sticky ends. The loop lengths of each motif are indicated in parentheses. The central strand (C), medium strands (M), and short strands (S) are colored blue/red, green, and black, respectively. Note that there are three red, central, single-stranded loops (L1, L2, and L3). The number of half-turns of the edge formed is labeled beside each branch. (b) Schematic illustration of the O-edge and E-edge. For the O-edge, neighboring motifs are related by a 2-fold rotational axis as indicated by a pair of black arrows. Light blue and purple hexagons indicate motifs facing up and down, respectively. (c–f) A set of four rules have been established to guide the design of DNA nanostructures.

nanostructures including a truncated square 2D lattice and three Archimedean solids: truncated octahedron, truncated cube, and truncated cuboctahedron, which are otherwise inaccessible from conventional symmetric designs. Please note that these rules point out only the general trends when comparing among different structures. The set of rules guides us to design a series of trial-and-error experiments from which the specific values for any particular structures are obtained.

RULES FOR THE TILE-BASED ASSEMBLY

Rule 1: The O-Edge Prohibits the Cyclization of Odd Numbers of Units, But the E-Edge Has No Such Restriction (Figure 1c). For an O-edge, two neighboring motifs are related by a 2-fold rotational symmetry (Figure 1b) and alternatively face up and down. Consequently, an even number of units is required to form a closed ring, and an odd number of units will confront face mismatch. For Motif-O, all three branches form the O-edge. This corrugated assembly pattern leads to a conflict in tile arrangement when motifs try to cyclize into a triangle, a pentagon, or any other polygons with an odd number of units (Figure S1). Motif-Es form E-edges and could potentially form any possible structure consisting of three-edge vertexes (Figure S3). As demonstrated previously (Table 1), several symmetric polyhedral structures containing an odd number of units within a polygonal face, such as the tetrahedron, the dodecahedron, and the truncated icosahedron, can be assembled only from Motif-E.[34] Nonetheless, the lack of limitation may lead to a low yield of the targeting structure because there are a large number of competing structures along the assembly pathway toward the target structure. Motif-EOE is a hybrid design with asymmetric branches. The cyclization between two branches forming E-edges, allows the formation of cyclized, oligomeric units with an arbitrary number of motifs. The protruding O-edges allow further cyclization of only even numbers of oligomeric units to form large assemblies (Figure S2). Motif-EOE provides better chances than Motif-E to form certain complex structures that are inaccessible from Motif-O, such as 2D lattices composing polygons with odd numbers of edges.

Rule 2: Long Central Loops Provide a High Degree of Out-of-Plane Flexibility (Figure 1d). Three single-stranded loops (red) are placed at the center of the motif and control the motif flexibility. Short loops introduce stress and thus rigidity into the motif to keep it planar, therefore facilitating the formation of flat 2D lattices or large closed structures. Long loops provide pronounced out-of-plane flexibility to allow the motif to significantly bend out-of-plane and favor the formation of small rather than large closed structures or a 2D lattice (Figure 1d). This rule is well illustrated by our previous study (Table 1), which demonstrates that Motif-E with 3-base-long loops forms a dodecahedron (containing 20 motifs) or a truncated icosahedron (containing 60 motifs), while the same motif with 5-base-long loops forms a small tetrahedron (containing 4 motifs).[35]

Rule 3: A Long Loop Allows a Small Interbranch Angle (Figure 1e). The single-stranded loop balances the flexibility and stress in the DNA motif according to our previous study.[45] In general, a long loop allows a small angle between its two flanking branches, and a short loop favors a large angle (Figure 1e). The optimal length of the single-stranded loop required for certain angles can be derived from our previous studies on symmetric motifs. Two- or 3-base-long loops and 4-base-long loops are optimal at 120° (as in hexagonal 2D arrays[27]) and 90° (as in tetragonal arrays[28]), respectively. A 3-base-long loop works well for angles of 108 and 120° as illustrated by the construction of dodecahedron and truncated icosahedron, respectively.[35] A 60° angle requires 5-base loops as in a tetrahedron.[35] If the loop length is far from the optimal length, then the yields of target structures significantly decrease.[45] However, longer loops can be deliberately used in certain cases. For instance, the targeting

DOI: 10.1021/jacs.6b06074
J. Am. Chem. Soc. 2016, 138, 13579–13585

Table 1. Summary of Structures Assembled from Three-Point-Star Motifs

structure	polygon	motif	loop (base)	DNA conc. (nM)	number of motifs	year
hexagonal 2D lattice	hexagon	Motif-O	3,3,3	600	N.A.	2005[27]
tetrahedron	triangle	Motif-E	5,5,5	75	4	2008[35]
dodecahedron	pentagon	Motif-E	3,3,3	50	20	2008[35]
truncated icosahedron	pentagon hexagon	Motif-E	3,3,3	500	60	2008[35]
cube	square	Motif-O Motif-E	5,5,5	50 200	8	2009[36]
triangular prism	triangle square	Motif-E	7,4,4	30−50	6	2012[42]
truncated square 2D lattice	square octagon	Motif-EOE	0,5,0 1,5,1	1000	N.A.	this study
truncated octahedron	square hexagon	Motif-O Motif-E	3,7,3 1,5,1	200 100	24	
truncated cube	triangle octagon	Motif-EOE	0,7,0	100	24	
truncated cuboctahedron	square hexagon octagon	Motif-0	1,5,1	1000	48	

structure is among the smallest closed structures that could be assembled. It is worth noting that, in the case of the asymmetric three-point-star motif, the flexibility/stress and thus interbranch angles of the motif are determined cooperatively by three single-stranded loops.

Rule 4: High DNA Concentration Favors Large Structure, but Low Concentration Promotes the Formation of Small Structures (Figure 1f). During DNA self-assembly, any existing DNA complex can either (1) incorporate more building motifs to grow into large complexes or (2) cyclize into closed complexes. At high DNA concentration, DNA complexes have high collision probabilities with individual motifs, leading to the formation of large complexes (Figure 1f). An example validating this rule comes from the assembly of a dodecahedron (20 motifs) and a truncated icosahedron (60 motifs) from Motif-E (3,3,3), which requires DNA concentrations of 50 nM and 500 nM, respectively.[35]

COMPLEX STRUCTURE CONSTRUCTION FROM ASYMMETRIC THREE-POINT-STAR MOTIFS

Retrosynthetic analysis is a powerful tool used in designing synthesis routes for complex organic molecules. A target molecule is transformed into simpler precursors, which in turn are transformed into even simpler precursors. The process is repeated until reaching simple, available precursors. We propose to apply the same process for nanostructure self-assembly or noncovalent nanostructure synthesis. We first demonstrated this approach by constructing a 2D, truncated square lattice that contained both squares and octagons. Such a complex lattice can be reduced to a simpler square-shaped unit. The 4-fold-symmetric unit can be further reduced into an even simpler asymmetric, three-branched structure, which can be realized by an asymmetric, three-point-star motif. The three interbranch angles in the star motif should be 90, 135, and 135° (Figure 2a). On the basis of the above established rules, the truncated square 2D lattice would require short loops (rule 2) and a high DNA concentration (rule 4), and one of the loops should have a length of roughly five bases to allow the formation of a 90° angle (rule 3). In addition, Motif-O and Motif-EOE would have a better chance than Motif-E (rule 1).

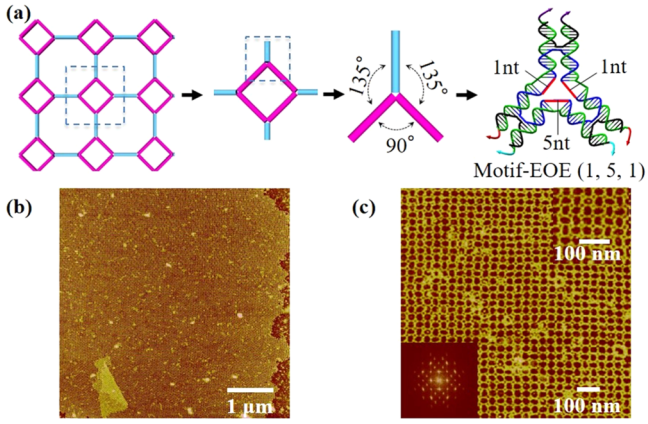

Figure 2. Truncated square 2D lattice assembled from Motif-EOE (1,5,1). (a) Retrosynthetic analysis of a truncated square 2D lattice. The 2D lattice is assembled from a simpler, 4-fold-symmetric unit, which in turn is assembled from an asymmetric three-point-star motif. A corresponding DNA motif is shown on the right. E-edge, purple; O-edge, cyan. (b) Large-area atomic force microscopy (AFM) image. (c) Small-area AFM image. Inset images illustrating a detailed pattern of the lattice and a fast Fourier transform pattern showing 4-fold symmetry.

On the basis of the above considerations, we used Motif-EOE (0,5,0) and (1,5,1) at a DNA concentration of 1 μM (Figure 2, Figure S8), which resulted in the desired 2D DNA arrays of up to tens of micrometers. AFM imaging revealed the detailed pattern of the arrays, and a fast Fourier transformation pattern showed 4-fold symmetry (Figure 2b,c). The observed repeating distance was 35.8 nm, in good agreement with the theoretical calculation of 35.2 nm assuming that the rise and diameter of B-duplex DNA are 0.33 nm/base pair and 2 nm, respectively. Lattices formed from Motif-EOE (2,5,2) hardly remained flat as single layers, suggesting that extra out-of-plane flexibility was induced by the elongated loops (Figure S8). With the same single-stranded loop lengths and DNA concentration, Motif-O and Motif-E failed to form a truncated square lattice. For Motif-O, this could be attributed to the competing effects from other structures (e.g., a truncated octahedron and a truncated cuboctahedron). Although such competing effects existed in

DOI: 10.1021/jacs.6b06074
J. Am. Chem. Soc. 2016, 138, 13579−13585

Motif-E as well, its high preference for curvature accumulation was a great challenge for 2D lattice formation. A 2D structure with a similar pattern had been realized by Zhang et al. with four different component three-point star motifs.[34] In comparison, only a one-component, three-point star motif was needed for the current approach.

We then constructed a 3D structure, a truncated octahedron, that was a relatively small polyhedron composed of 24 motifs with 6 squares and 8 hexagons. The three interbranch angles at each vertex were 90, 120, and 120° (Figure 3a). According to rule 1, formation of the truncated octahedron was prohibited with Motif-EOE, while not with Motif-O or Motif-E. On the basis of rules 2 and 4, long single-stranded loops and a low DNA concentration should be used in order to promote the formation of small closed structures. And one loop should have a minimal length of five bases to allow the formation of a 90° angle (rule 3). Thus, we tested Motif-O (3,7,3) with a DNA concentration of 200 nM (Figure 3) and Motif-E (1,5,1) with a DNA concentration of 100 nM (Figures S11 and S12). Both of them successfully self-assembled into the truncated octahedron. The relative short loop of Motif-E might be due to its ease of curvature accumulation. A truncated octahedron constructed from Motif-O was presented in Figure 3. Gel electrophoresis confirmed the formation of a dominant DNA complex with a mobility slower than that of the DNA cube (Figure 3b). The assembly yield was estimated to be 53% based on the band intensity. AFM imaging shows that the DNA complex had a size (measured diameter, 63.6 ± 2.4 nm; theoretical diameter, 64.4 nm) and 2D projections expected for a truncated octahedron (Figure 3c and Figure S9). Many unclosed structures are observed on AFM images. The heterogeneity seems more severe on AFM images than on gel electrophoresis potentially because (1) flat, nonclosed structures have higher adsorption onto the mica substrate; (2) 3D structures got broken while being deposited onto the mica substrate or during the imaging process because of the mechanical interference by the AFM tip. To unambiguously reveal the 3D configuration of the DNA complex, we utilized cryoEM imaging in conjunction with single-particle 3D reconstruction. A representative raw cryoEM micrograph was presented in Figure 3d, in which individual particles with similar size and 2D projections to the truncated octahedron could be easily found. From selected raw particles, the 3D model was reconstructed (Figure 3e). We further compared 2D projections of the reconstructed 3D model with raw particles (Figure 3f, Figure S10). The pairwise comparison revealed a clear similarity, indicating that the reconstructed model indeed represented the true 3D configuration of the truncated octahedron.

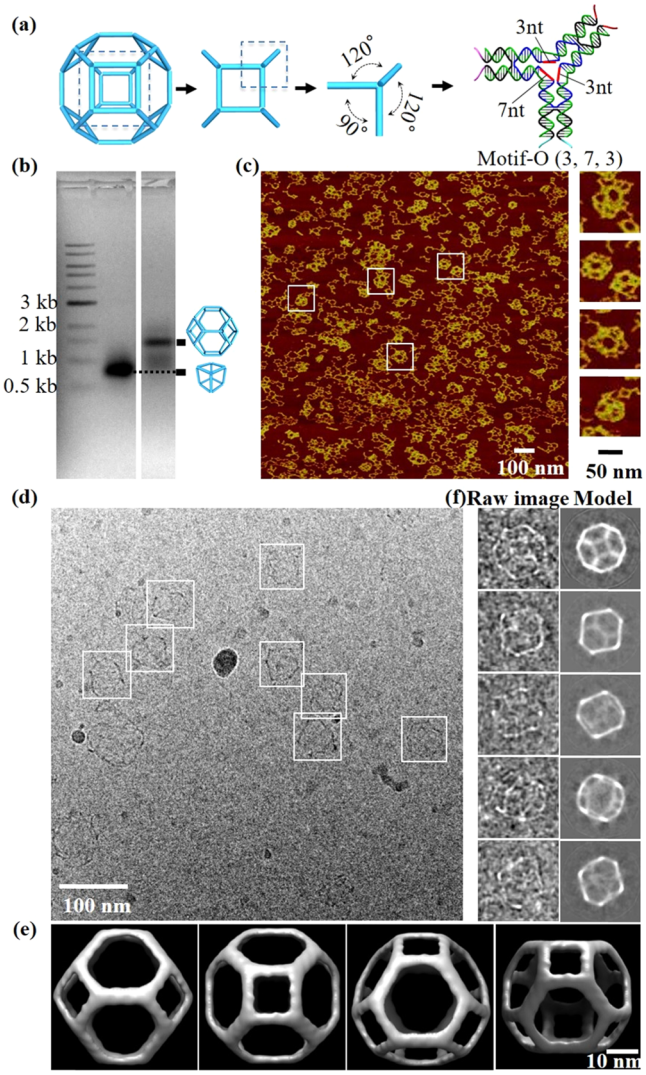

Figure 3. Truncated octahedron assembled from Motif-O (3,7,3). (a) Retrosynthetic analysis of a truncated octahedron. (b) Native agarose gel analysis of Motif-O (3,7,3) assembly. A DNA cube assembled from Motif-O (5,5,5) is used as the reference in lane 2. (c) AFM imaging of the truncated octahedron. Particles that have similar projections onto the structural model of the truncated octahedron are highlighted in white boxes and presented in the right panel. (d) Representative cryoEM image of the truncated octahedron. White boxes indicate the DNA particles. (e) Four views of the reconstructed structural model of the truncated octahedron. (f) Pairwise comparison between raw cryoEM images of individual particles (left) and the corresponding projections (right) of the reconstructed structural model. The raw particles were selected from different image frames to represent views at different orientations.

Our next target 3D structure was a truncated cube, which consisted of eight triangles and six octagons. The three interbranch angles at each vertex were 60, 135, and 135° (Figure 4a). Motif-O was excluded because the triangle contained an odd number of edges (rule 1). The truncated cube had similar curvature and size (24 motifs) of those of the truncated octahedron but with a smaller interbranch angle of 60°, which suggested a slightly enhanced loop asymmetry while keeping similar out-of-plane flexibility and DNA concentration (rules 2−4). At the end, a truncated cube was assembled from Motif-EOE (0,7,0) with a DNA concentration of 100 nM (Figure 4), whereas Motif-E failed to produce the truncated cube (Figure S3). For Motif-EOE, its intrinsic geometrical limitation helped to prevent the formation of competing structures such as a truncated octahedron, but Motif-E had no such advantage of eliminating competing structures. Center loops of (0,7,0) provided a large amount of stress in order to form the triangle unit needed for truncated cube construction, which resulted in limited out-of-plane motif flexibility and thus a high tendency to form large assemblies at high DNA concentration as shown in the gel (Figure S5), which explained why a low DNA concentration (100 nM) was needed for the construction of the truncated cube. The successful formation of the truncated cube was confirmed by gel electrophoresis (yield 66%), AFM imaging, and cryoEM imaging (Figure 4, Figures S13−S15).

DOI: 10.1021/jacs.6b06074
J. Am. Chem. Soc. 2016, 138, 13579−13585

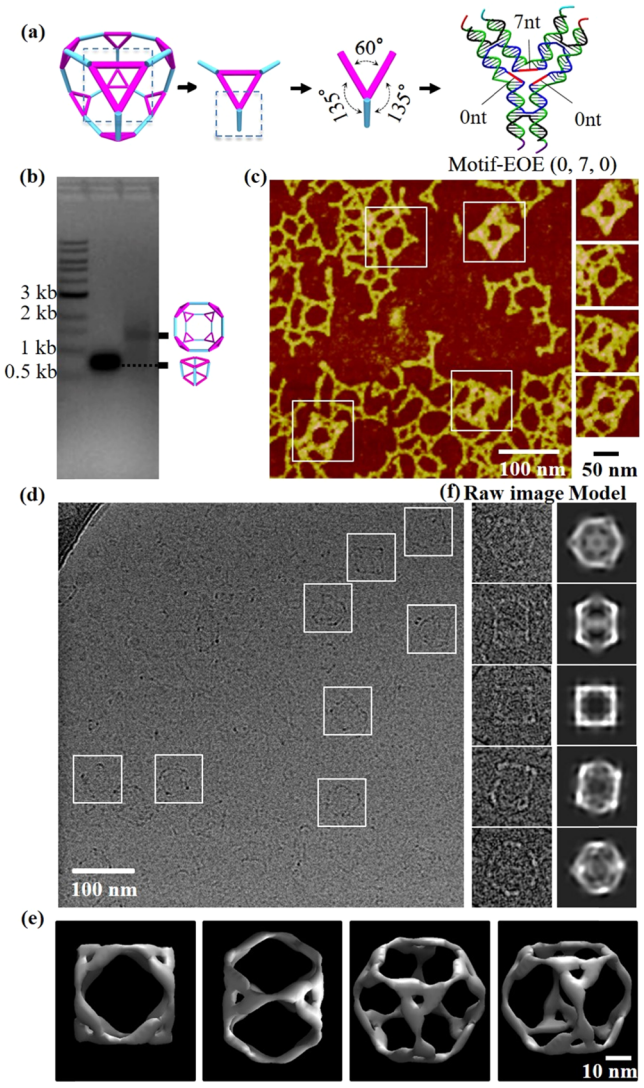

Figure 4. Truncated cube assembled from Motif-EOE (0,7,0). (a) Retrosynthetic analysis of a truncated cube. (b) Native agarose gel analysis of Motif-EOE (0,7,0) assembly. A DNA cube assembled from Motif-EOE (5,5,5) is used as reference in lane 2. For the schematics, E-edge, purple; O-edge, cyan. (c) AFM imaging of the truncated cube. Particles that have projections similar to the structural model of the truncated octahedron are highlighted in white boxes and presented in the right panel. (d) A representative cryoEM image of the truncated cube. White boxes indicate the DNA particles. (e) Four views of the reconstructed structural model of the truncated octahedron. (f) Pairwise comparison between raw cryoEM images of individual particles (left) and the corresponding projections (right) of the reconstructed structural model.

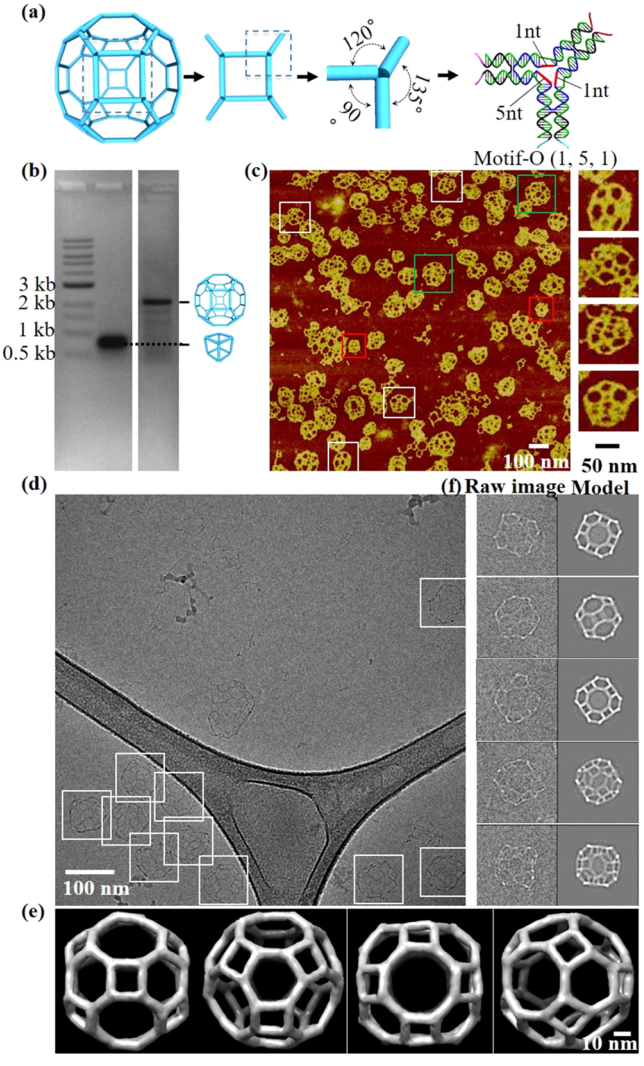

Figure 5. Truncated cuboctahedron assembled from Motif-O (1,5,1). (a) Retrosynthetic analysis of a truncated cuboctahedron. (b) Native agarose gel analysis of Motif-O (1,5,1) assembly. A DNA cube assembled from Motif-O (5,5,5) is used as reference in lane 2. (c) AFM imaging of the truncated cuboctahedron. Particles that have projections similar to the structural model of the truncated cuboctahedron are highlighted in white boxes and presented in the right panel. Two other populations of nanocages with different sizes are highlighted in green and red boxes. (d) Representative cryoEM image of the truncated cuboctahedron. White boxes indicate the DNA particles. (e) Four views of the reconstructed structural model of the truncated cuboctahedron. (f) Pairwise comparison between raw cryoEM images of individual particles (left) and the corresponding projections (right) of the reconstructed structural model. The raw particles were selected from different image frames to represent views with different orientations.

Finally, we constructed a more complex 3D structure, a truncated cuboctahedron. It consisted of 48 motifs and 3 different polygonal faces: 12 squares, 8 hexagons, and 6 octagons (Figure 5a). Similar to the truncated octahedron, Motif-EOE lacked the capability to form the truncated cuboctahedron (rule 1). The three interbranch angles at each vertex were 90, 120, and 135°, which added up to 345°, indicating the minimal requirement for out-of-plane flexibility and thus short loops (rule 2). The longest loop should have a minimal length of five bases to fulfill the requirement of forming an interbranch angle of 90° (rule 3). The truncated cuboctahedron contains 48 motifs, which doubled the sizes of a truncated octahedron (containing 24 motifs) and a truncated cube (containing 24 motifs), suggesting that a high DNA concentration might be necessary (rule 4). As anticipated, a truncated cuboctahedron was successfully constructed from Motif-O, with center loop lengths of (1,5,1) and a DNA concentration of 1 μM (Figure 5). Native agarose gel electrophoresis showed a dominant band (yield 51%) with retarded mobility compared to that of a DNA cube [assembled from Motif-O (5,5,5), Figure 5b]. AFM imaging confirmed the formation of nanocages with minimal flat structures observed,

DOI: 10.1021/jacs.6b06074
J. Am. Chem. Soc. 2016, 138, 13579−13585

potentially due to the fact that they are more stable than a truncated octahedron and a truncated cube because they are larger and do not need to bend out of plane significantly; they are also subject to a weaker shearing force while depositing onto the mica surface. The dominant population of nanocages had a relatively uniform size (93.2 ± 5.6 nm), close to the predicted diameter (87.0 nm) of the truncated cuboctahedron (Figure 5c). AFM images of particles with similar 2D projections of a truncated cuboctahedron were highlighted in white boxes and are presented in the right panel of Figure 5b. In addition to the truncated cuboctahedron, other two populations of nanocages could be observed in AFM images (Figure 5c, Figure S16). The large nanocage (highlighted in green boxes) had a diameter of 123.1 ± 9.5 nm (presumably a truncated icosidodecahedron), and the small one (highlighted in red boxes) had a diameter of 63.4 ± 3.9 nm (presumably a truncated octahedron). Unambiguous confirmation of the formation of the truncated cuboctahedron came from cryoEM imaging and 3D reconstruction (Figure 5d–f, Figure S17). Reconstruction of the suspected truncated icosidodecahedron and truncated octahedron was not accomplished because of a limited number of particles of these two populations from cryoEM imaging.

CONCLUSIONS

We have developed a retrosynthetic analysis for designing routes to assemble complex DNA nanostructures and have established a set of four basic rules for DNA tile-based self-assembly. They could serve as general guidelines for designing DNA nanostructures. Along with previous studies, these rules have been validated in the current study via introducing asymmetry into three-point-star motifs to generate a series of 2D and 3D structures with moderate complexity. We should note that the presented strategy here has its advantages and limitations in terms of the scope of nanostructures that it can construct. (1) Symmetry. The strategy relies on structural symmetries. The intrinsic overall symmetries allow us to dissect a complex structure into multiple copies of identical and small DNA nanomotifs. Thus, this strategy can produce only structures with high overall symmetries and cannot produce structures with no symmetry. (2) Size. We do not see any intrinsic size limitation with this method. However, the size heterogeneity will become a more and more serious issue when the size of the target structures goes up, particularly when the overall size is over 100 nm. (3) Shape. Because of the symmetry requirement, this strategy can produce only simple or moderately complex structures, such as 2D period arrays, 1D nanotubes, and polyhedra. Clearly, complex structures and patterns, such as the America map produced by the DNA origami approach,[12] is beyond the capability of this strategy. (4) Tile. This strategy is demonstrated with, but should not be limited to, the three-point-star motif. It would be quite straightforward to apply to other point-star motifs. It is also conceivable to apply it to other large DNA tiles, such as origami tiles. (5) Other approaches. Similar structures could be constructed by other methods, such as origami. However, origami structures and single-strand tile (SST) structures[22] are intrinsically asymmetric, whereas our structures are intrinsically symmetric. In general, origami structures are expected to be more geometrically stable than SST structures and our structures because long, scaffold, single DNA strands go through entire structures. But all of the DNA strands in our structures and SST structures are held together by only base pairing. Beyond the intellectual development in structural DNA nanotechnology of this strategy, the reported structures might also find some technological applications, such as encapsulating agents, organizing scaffolds, and hubs for preparing multivalent ligands.

ASSOCIATED CONTENT

Supporting Information

The Supporting Information is available free of charge on the ACS Publications website at DOI: 10.1021/jacs.6b06074.

Experimental methods and additional experimental data (PDF)

AUTHOR INFORMATION

Corresponding Authors

*E-mail: wanggs2003@hotmail.com.
*E-mail: mao@purdue.edu.

Author Contributions

P.W., S.W., and C.T. contributed equally.

Notes

The authors declare no competing financial interest.

ACKNOWLEDGMENTS

We thank the NSF (no. 1437301), NSFC (no. 81429001), and ONR (N00014-15-1-2702) for their support of this work.

REFERENCES

(1) Seeman, N. C. *Nature* **2003**, *421*, 427–431.
(2) Tian, Y.; Wang, T.; Liu, W. Y.; Xin, H. L.; Li, H. L.; Ke, Y. G.; Shih, W. M.; Gang, O. *Nat. Nanotechnol.* **2015**, *10*, 637–644.
(3) Schreiber, R.; Do, J.; Roller, E.-M.; Zhang, T.; Schuller, V. J.; Nickels, P. C.; Feldmann, J.; Liedl, T. *Nat. Nanotechnol.* **2014**, *9*, 74–78.
(4) Kuzyk, A.; Schreiber, R.; Zhang, H.; Govorov, A. O.; Liedl, T.; Liu, N. *Nat. Mater.* **2014**, *13*, 862–866.
(5) Ko, S. H.; Liu, H. P.; Chen, Y.; Mao, C. D. *Biomacromolecules* **2008**, *9*, 3039–3043.
(6) Li, J.; Pei, H.; Zhu, B.; Liang, L.; Wei, M.; He, Y.; Chen, N.; Li, D.; Huang, Q.; Fan, C. H. *ACS Nano* **2011**, *5*, 8783–8789.
(7) Walsh, A. S.; Yin, H. F.; Erben, C. M.; Wood, M. J. A.; Turberfield, A. J. *ACS Nano* **2011**, *5*, 5427–5432.
(8) Douglas, S. M.; Bachelet, I.; Church, G. M. *Science* **2012**, *335*, 831–834.
(9) Jiang, Q.; Song, C.; Nangreave, J.; Liu, X. W.; Lin, L.; Qiu, D. L.; Wang, Z. G.; Zou, G. Z.; Liang, X. J.; Yan, H.; Ding, B. Q. *J. Am. Chem. Soc.* **2012**, *134*, 13396–13403.
(10) Lee, H.; Lytton-Jean, A. K. R.; Chen, Y.; Love, K. T.; Park, A. I.; Karagiannis, E. D.; Sehgal, A.; Querbes, W.; Zurenko, C. S.; Jayaraman, M.; Peng, C. G.; Charisse, K.; Borodovsky, A.; Manoharan, M.; Donahoe, J. S.; Truelove, J.; Nahrendorf, M.; Langer, R.; Anderson, D. *Nat. Nanotechnol.* **2012**, *7*, 389–393.
(11) Zhao, Y. X.; Shaw, A.; Zeng, X. H.; Benson, E.; Nystrom, A. M.; Hogberg, B. *ACS Nano* **2012**, *6*, 8684–8691.
(12) Rothemund, P. W. K. *Nature* **2006**, *440*, 297–302.
(13) Dietz, H.; Douglas, S. M.; Shih, W. M. *Science* **2009**, *325*, 725–730.
(14) Douglas, S. M.; Dietz, H.; Liedl, T.; Hogberg, B.; Graf, F.; Shih, W. M. *Nature* **2009**, *459*, 414–418.
(15) Han, D. R.; Pal, S.; Nangreave, J.; Deng, Z. T.; Liu, Y.; Yan, H. *Science* **2011**, *332*, 342–346.
(16) Han, D. R.; Pal, S.; Yang, Y.; Jiang, S. X.; Nangreave, J.; Liu, Y.; Yan, H. *Science* **2013**, *339*, 1412–1415.
(17) Iinuma, R.; Ke, Y. G.; Jungmann, R.; Schlichthaerle, T.; Woehrstein, J. B.; Yin, P. *Science* **2014**, *344*, 65–69.

DOI: 10.1021/jacs.6b06074
J. Am. Chem. Soc. 2016, 138, 13579–13585

(18) Benson, E.; Mohammed, A.; Gardell, J.; Masich, S.; Czeizler, E.; Orponen, P.; Hogberg, B. *Nature* **2015**, *523*, 441−444.
(19) Zhang, F.; Jiang, S.; Wu, S.; Li, Y.; Mao, C.; Liu, Y.; Yan, H. *Nat. Nanotechnol.* **2015**, *10*, 779−784.
(20) Ke, Y. G.; Ong, L. L.; Shih, W. M.; Yin, P. *Science* **2012**, *338*, 1177−1183.
(21) Ke, Y. G.; Ong, L. L.; Sun, W.; Song, L.; Dong, M. D.; Shih, W. M.; Yin, P. *Nat. Chem.* **2014**, *6*, 994−1002.
(22) Wei, B.; Dai, M. J.; Yin, P. *Nature* **2012**, *485*, 623−626.
(23) Ke, Y. G.; Liu, Y.; Zhang, J. P.; Yan, H. *J. Am. Chem. Soc.* **2006**, *128*, 4414−4421.
(24) Mitchell, J. C.; Harris, J. R.; Malo, J.; Bath, J.; Turberfield, A. J. *J. Am. Chem. Soc.* **2004**, *126*, 16342−16343.
(25) Rothemund, P. W. K.; Ekani-Nkodo, A.; Papadakis, N.; Kumar, A.; Fygenson, D. K.; Winfree, E. *J. Am. Chem. Soc.* **2004**, *126*, 16344−16352.
(26) Liu, H. P.; Chen, Y.; He, Y.; Ribbe, A. E.; Mao, C. D. *Angew. Chem., Int. Ed.* **2006**, *45*, 1942−1945.
(27) He, Y.; Chen, Y.; Liu, H. P.; Ribbe, A. E.; Mao, C. D. *J. Am. Chem. Soc.* **2005**, *127*, 12202−12203.
(28) He, Y.; Tian, Y.; Chen, Y.; Deng, Z. X.; Ribbe, A. E.; Mao, C. D. *Angew. Chem., Int. Ed.* **2005**, *44*, 6694−6696.
(29) Liu, H. P.; He, Y.; Ribbe, A. E.; Mao, C. D. *Biomacromolecules* **2005**, *6*, 2943−2945.
(30) He, Y.; Tian, Y.; Ribbe, A. E.; Mao, C. D. *J. Am. Chem. Soc.* **2006**, *128*, 15978−15979.
(31) Winfree, E.; Liu, F. R.; Wenzler, L. A.; Seeman, N. C. *Nature* **1998**, *394*, 539−544.
(32) Yan, H.; Park, S. H.; Finkelstein, G.; Reif, J. H.; Labean, T. H. *Science* **2003**, *301*, 1882−1884.
(33) Zhang, F.; Liu, Y.; Yan, H. *J. Am. Chem. Soc.* **2013**, *135*, 7458−7461.
(34) Zhang, F.; Jiang, S. X.; Li, W.; Hunt, A.; Liu, Y.; Yan, H. *Angew. Chem., Int. Ed.* **2016**, *55*, 8860−8863.
(35) He, Y.; Ye, T.; Su, M.; Zhang, C.; Ribbe, A. E.; Jiang, W.; Mao, C. D. *Nature* **2008**, *452*, 198−201.
(36) Zhang, C.; Ko, S. H.; Su, M.; Leng, Y. J.; Ribbe, A. E.; Jiang, W.; Mao, C. D. *J. Am. Chem. Soc.* **2009**, *131*, 1413−1415.
(37) Zheng, J. P.; Birktoft, J. J.; Chen, Y.; Wang, T.; Sha, R. J.; Constantinou, P. E.; Ginell, S. L.; Mao, C. D.; Seeman, N. C. *Nature* **2009**, *461*, 74−77.
(38) He, Y.; Su, M.; Fang, P. A.; Zhang, C.; Ribbe, A. E.; Jiang, W.; Mao, C. D. *Angew. Chem., Int. Ed.* **2010**, *49*, 748−751.
(39) Li, X.; Zhang, C.; Hao, C. H.; Tian, C.; Wang, G. S.; Mao, C. D. *ACS Nano* **2012**, *6*, 5138−5142.
(40) Tian, C.; Li, X.; Liu, Z. Y.; Jiang, W.; Mao, C. D. *Angew. Chem., Int. Ed.* **2014**, *53*, 8041−8044.
(41) Zhang, C.; Su, M.; He, Y.; Zhao, X.; Fang, P. A.; Ribbe, A. E.; Jiang, W.; Mao, C. D. *Proc. Natl. Acad. Sci. U. S. A.* **2008**, *105*, 10665−10669.
(42) Zhang, C.; Wu, W. M.; Li, X.; Tian, C.; Qian, H.; Wang, G. S.; Jiang, W.; Mao, C. D. *Angew. Chem., Int. Ed.* **2012**, *51*, 7999−8002.
(43) Goodman, R. P.; Berry, R. M.; Turberfield, A. J. *Chem. Commun.* **2004**, *7*, 1372−1373.
(44) Edwardson, T. G. W.; Carneiro, K. M. M.; Mclaughlin, C. K.; Serpell, C. J.; Sleiman, H. *Nat. Chem.* **2013**, *5*, 868−875.
(45) He, Y.; Mao, C. D. *Chem. Commun.* **2006**, *9*, 968−969.

DOI: 10.1021/jacs.6b06074
J. Am. Chem. Soc. 2016, 138, 13579−13585